Integrated numerical simulations and modelling of erosion and deposition on plasma facing walls

Kaoru Ohya

Institute of Technology and Science, The University of Tokushima, Japan

Contributions from K. Inai[1], A. Kirschner[2], A. Ito[3], G. Kawamura[3], H. Nakamura[3], Y. Tomita[3] and T. Tanabe[4]

[1]Institute of Technology and Science, The University of Tokushima, Japan
[2]Institut fuer Energieforschung-Plasmaphysik, Forschungszentrum Juelich, Germany
[3]Department of Simulation Science, National Institute for Fusion Science, Japan
[4]Interdisciplinary Graduate School of Engineering, Kyushu University, Japan

Outline

(A) INTRODUCTION TO EROSION/DEPOSITION

a) Related issues to erosion/deposition

b) Modelling of erosion/deposition

c) Simulation codes for plasma wall interactions

(B) MODELLING AND INTEGRATED SIMULATIONS

a) Projectile reflection and physical sputtering

b) Chemical sputtering and hydrocarbon emission

c) Impurity deposition and collisional mixing

d) Thermal diffusion of impurities in materials

e) Impurity transport in near-surface plasmas

f) Molecular dynamics simulation of particle solid interactions

g) Particle-in-cell simulation of plasma/sheath on surfaces

(A) INTRODUCTION TO EROSION/DEPOSITION

a) Related issues to erosion/deposition

b) Modeling of erosion/deposition

c) Simulation codes for plasma wall interactions

a) Related Issues to Erosion/Deposition in Fusion Devices

(1) Erosion of wall elements

Reduced life time of wall elements

(2) Eroded impurities can penetrate into the plasma

Dilution and radiation cooling of core plasma

(3) Redeposition of eroded impurities

Tritium retention in redeposited layers

Erosion, transport and redeposition of impurities is a crucial issue in fusion devices !

b) Modeling of Erosion/Deposition of Plasma Facing Walls

Carbon based materials for PFW

Key issues:
Chemical sputtering & Tritium incorporation

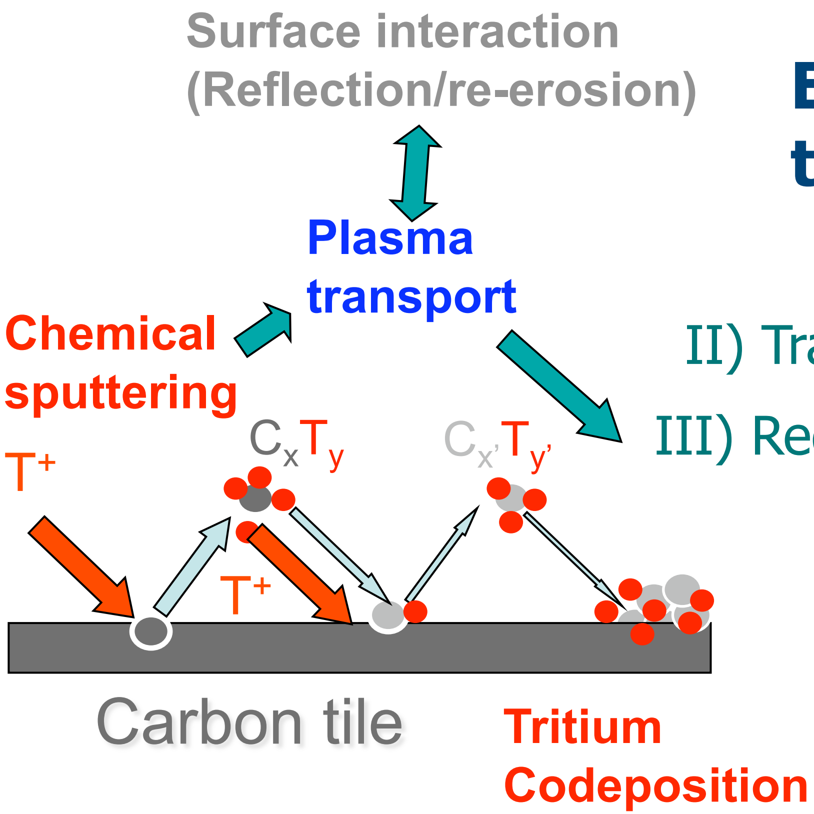

Erosion/deposition codes require to treat self-consistently:

I) Physical and chemical erosion ***of*** surface

II) Transport of released impurities ***above*** surface

III) Redeposition of returning impurities ***on*** surface

IV) Resultant material mixing ***below*** surface

Integrated simulation of erosion/deposition is NEEDED

c) Simulation Codes for Plasma Wall Interactions

(A) Ion-Solid Interactions —reflection, erosion, material mixing—

1) TRIM (static-MC, J.P.Biersack, L.G.Haggmark, Nucl.Instr.Meth. 174 (1980) 257)
2) ACAT (static-MC, Y.Yamamura, Y.Mizuno, IPPJ-AM-40 Nagoya Univ. (1985))

3) TRIDYN (dynamic-MC, W.Moller, W.Eckstein, Nucl.Instr.Meth.B 2 (1984) 814)
4) ACAT-DIFFUSE (dynamic-MC, Y.Yamamura, Nucl.Instr.Meth. B 28 (1987) 17)
5) EDDY (dynamic- and static-MC, K.Ohya et al., Jpn.J.Appl.Phys. 35 (1996) 4523; Rad. Eff Def. Sol.142 (1997) 401)

6) HCParcas (classical-MD, E.Salonen, K.Nordlund et al., Europhys.Lett. 52 (2000) 504)
7) MolDyn (classical-MD, D.A.Alman, D.N.Ruzic, J. Nucl.Mater. 313-316 (2003) 182)
8) Classical-MD : J.Marian e.al., J.Appl. Phys. 101(2007) 044506
9) Classical-MD : P.S. Krstic et al., New J.Phys., 9 (2007) 209.
10) Classical-MD : K.Inai, Y.Kikuhara, K.Ohya, Surf. Coat. Technol., 22-23 (2008) 5374.
11) Classical-MD : Z. Yang et al., J. Nucl. Mater. 390-391(2009)136.

(B) local deposition —Impurity transport in near-surface plasmas—

1) WBC (3D-MC, J.N.Brooks, Phys.Fluids B 2 (1990) 1858)
2) ERO (2/3D-MC, D.Naujoks et al., Nucl. Fusion 33 (1993) 581; U.Koegler et al., Report Jul-3361, juelich, 1997; A.Kirschner et al., Nucl. Fusion 40 (2000) 1421)
3) DIVIMP (2D-MC, P.C.Stangeby et al., J.Nucl.Mater. 196-198 (1992) 258)
4) EDDY (3D-MC, J.Kawata, K. Ohya, Jpn.J.Appl.Phys. 34 (1995) 6237)

(B) MODELLING AND INTEGRATED SIMULATION

a) Projectile reflection and physical sputtering

b) Chemical sputtering and hydrocarbon emission

c) Impurity deposition and collisional mixing

d) Thermal diffusion of impurities in materials

e) Impurity transport in near-surface plasmas

f) Molecular dynamics simulation of particle solid interactions

g) Particle-in-cell simulation of plasma/sheath on surfaces

a) Projectile Reflection and Physical Sputtering

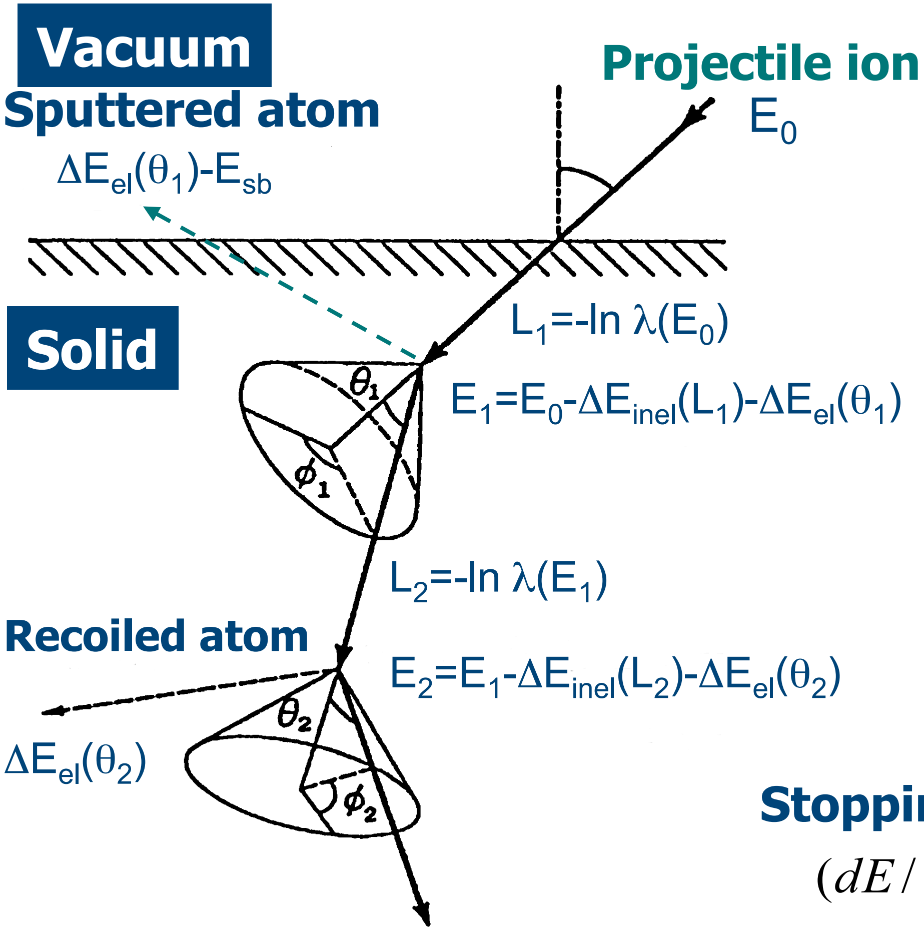

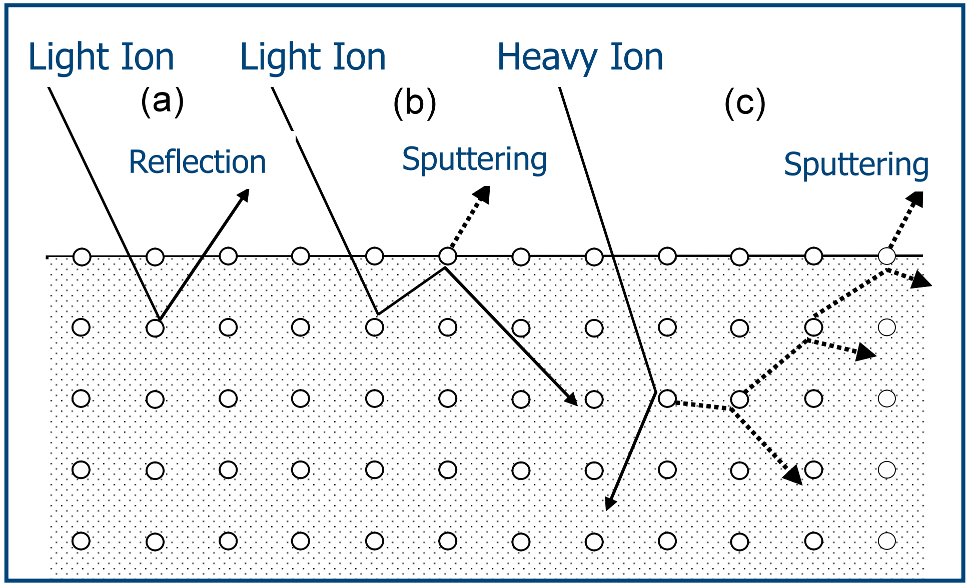

Analytic formula for scattering angle :

$$\cos\frac{\theta}{2}=\frac{b+\rho+\Delta}{\xi_c+\rho}$$

Stopping power:

$$(dE/dx)_{nonlocal}=1.212\frac{Z_a^{7/6}Z_b}{\left(Z_a^{2/3}+Z_b^{2/3}\right)^{3/2}}\sqrt{E}\quad\left[eV\cdot\text{Å}^2\right]$$

Energy of sputtered atoms:

$$E=E'-E_{sb}$$

Emission angle of Sputtered atoms :

$$\cos\beta=\sqrt{\frac{E'\cos^2\beta'-E_s}{E'-E_s}}$$

b) Chemical Sputtering and hydrocarbon emission

Hydrogen ion penetrates into carbon and forms hydrocarbon after thermalization, which diffuses to surface and desorbs.

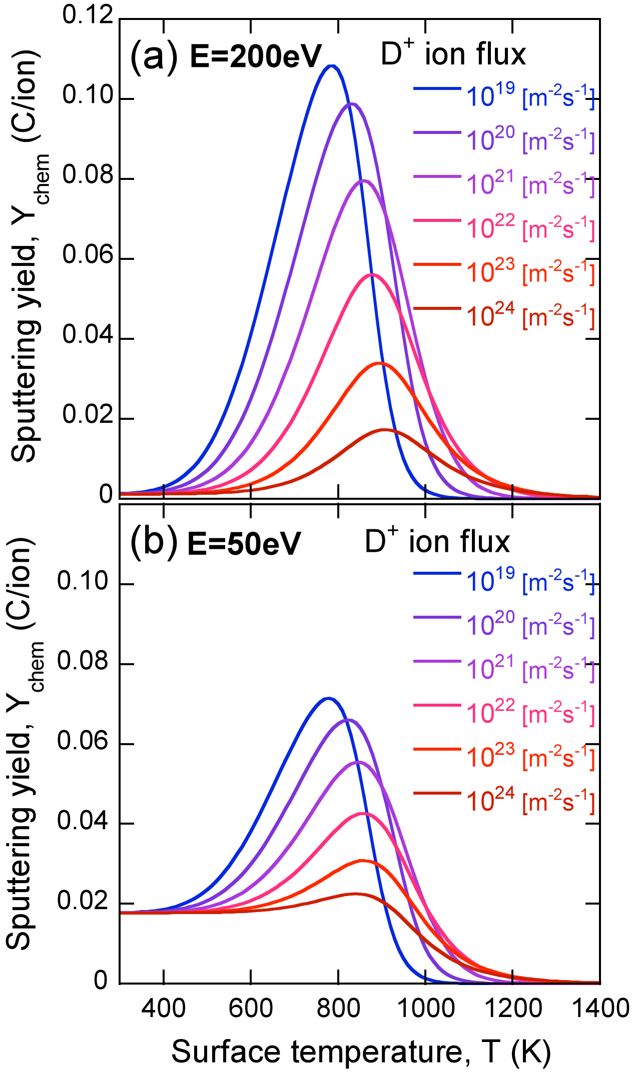

Formalization by Roth [JNM266-269(199)51] :

$$Y_{chem}(E,T,\varphi) = \frac{Y_{low}(E,T)}{1+\left(\dfrac{\phi}{6\times10^{21}}\right)^{0.54}}$$

$$Y_{low} = Y_{therm}(1 + DY_{dam}) + Y_{surf}$$

Y_{therm}: chemical erosion by thermalized ions

Y_{dam}: enhancement of thermal erosion by radiation damage

Y_{surf}: ion induced desorption of hydrocarbon radicals

Sputtering yield strongly depends on surface temperature (**T**) and energy (**E**) and ion flux (ϕ) of bombarding ions

c) Impurity Deposition and Collisional Mixing

Differential Fluence: $\Delta\Phi = \Phi / N_H$ (Φ: Total fluence, N_H : Number of pseudo ions)

Surface Thickness: $d = \sum_{i=1}^{N} \Delta x_i$ (N : Number of layers, Δx_i : i-th Layer thickness)

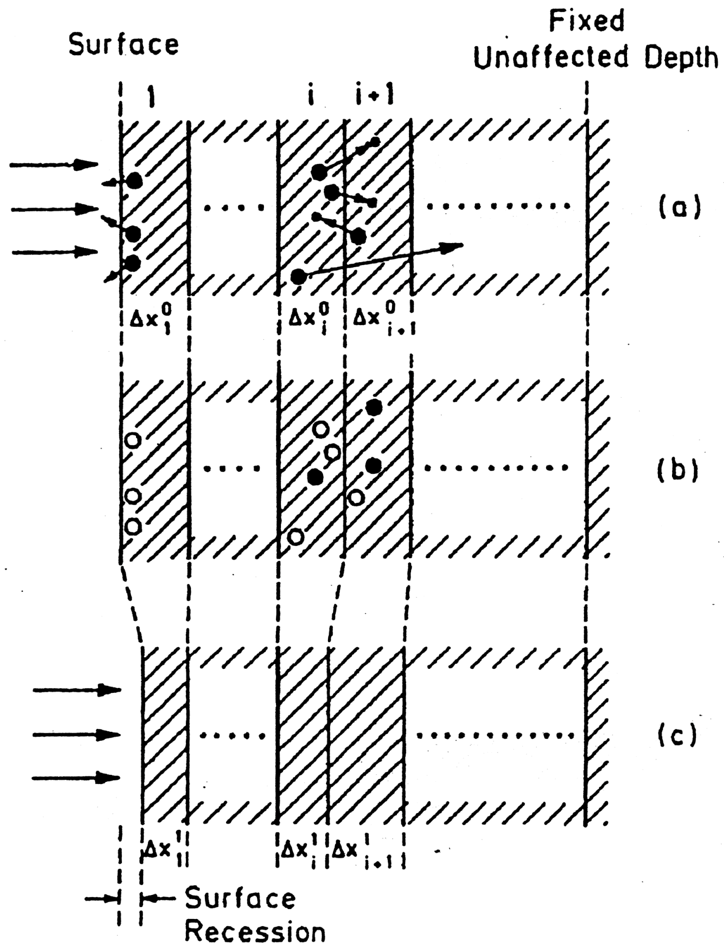

Collision process of a pseudo Ion :

Reflection, Implantation, Physical Sputtering

After simulation of collision process :

Areal density of j-th atom in i-th layer :

$$A_{ij} = q_j n_i \Delta x_i + \Delta N_{ij} \Delta\Phi$$

(ΔN_{ij}: Change in number of j-th atom in i-th layer)

i-th layer thickness : $\Delta x_i = \sum_{j=1}^{N_c} A_{ij} n_{0,j}^{-1}$ ($n_{0,j}$: j-th atom density)

j-th atom constituent in i-th layer : $q_{ij} = A_{ij} / \sum_{k=1}^{N_c} A_{ik}$

Maximum areal density of 1th atom in i-th layer : $A_{i1}^{\max} = [q_1^{\max} / (1 - q_1^{\max})] \sum_{j=2}^{N_c} A_{ij}$

$$\left.\begin{array}{ll} \text{Reemission} & \Delta A_{i1}^{reem} = A_{i1} - A_{i1}^{\max} \\ \text{Saturation} & A_{i1} = A_{i1}^{\max} \end{array}\right\} A_{i1} > A_{i1}^{\max}$$

d) Thermal Diffusion of Implanted Impurities

(1st)

$\Delta\phi \rightarrow$ EDDY

$\Delta t = \Delta\phi / \Gamma$

(1st)

$$\frac{\partial C(x,t)}{\partial t} = D \frac{\partial^2 C(x,t)}{\partial^2 x}$$

(2nd)

$\Delta\phi \rightarrow$ EDDY

$\Delta t = \Delta\phi / \Gamma$

(Nth)

$$\frac{\partial C(x,t)}{\partial t} = D \frac{\partial^2 C(x,t)}{\partial^2 x}$$

★ Impurity Deposition and Collisional Mixing

★ Thermal Diffusion of Deposited Impurities

Diffusion Coefficient $D = D_0 \exp(-Q_D / kT)$

D_0 : Material Constant (cm^2s^{-1})

Q_D : Activation Energy (eV)

T : Material Temperature (K)

Γ : Incident Ion Flux ($cm^{-2}s^{-1}$)

ϕ : Total Ion Fluence (cm^{-2})

t : $(= \phi / \Gamma)$ Irradiation Time (s)

N : Number of Pseudo Ions

$\Delta\phi$: $(= \phi / N)$ Differential Ion Flux (cm^{-2})

Δt : $(= t / N)$ Differential Irradiation time (s)

(B) MODELLING AND INTEGRATED SIMULATION

a) Projectile reflection and physical sputtering

b) Chemical sputtering and hydrocarbon emission

c) Impurity deposition and collisional mixing

d) Thermal diffusion of impurities in materials

e) Impurity transport in near-surface plasmas

f) Molecular dynamics simulation of particle solid interactions

g) Particle-in-cell simulation of plasma/sheath on surfaces

Monte Carlo Modeling of Impurity Transport

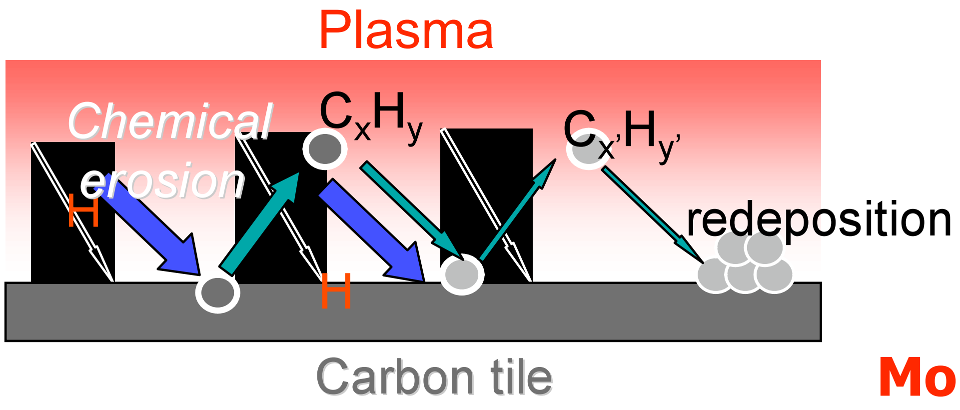

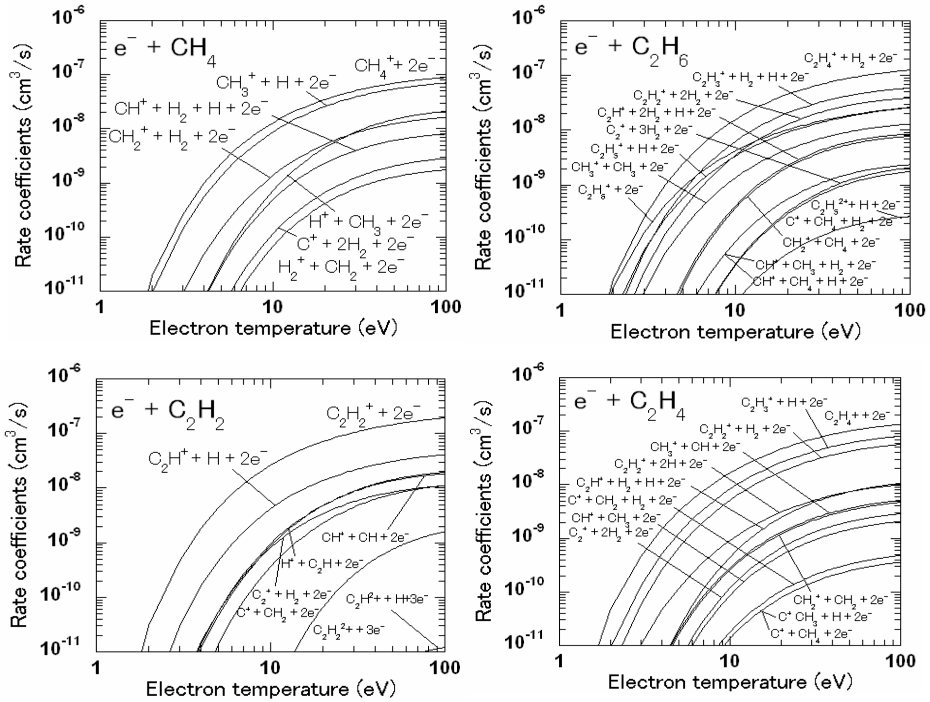

- The released C_xH_y molecule successively collides with plasma electrons and ions.

More than 700 reactions are included.

(R.K.Janev, D.Reiter, Rep.FZ-Juelich, Jul-3966(2002); Jul-4005 (2003))

- The elastic collisions with the **residual neutral hydrogen atoms**

T. Motohiro, Y. Taga, Thin Solid Films, 112 (1984) 161.

The model includes

- Lorenz force $F_z = q(v \times B)$
- friction force and
  temperature gradient thermal force

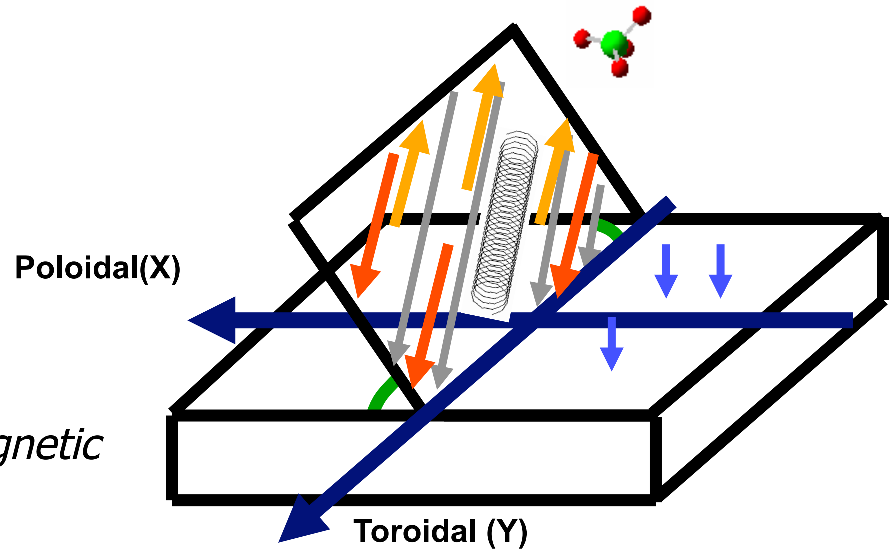

: P.C.Stangeby, *The Plasma Boundary of Magnetic Fusion Devices* (IOP, Bristol, 2000) p.296.

- Debye sheath and magnetic pre-sheath potential

ϕ_0 : sheath potential

: J.N.Brooks, Phys. Fluids B2(1990)1858.

- Cross-field diffusion

$D_\perp = 1 \ [m^2/s]$: K. Shimizu, T. Takizuka purakakugakkaishi 71 (1995) 1135.

Hydrocarbon Redeposition on PFW Surfaces

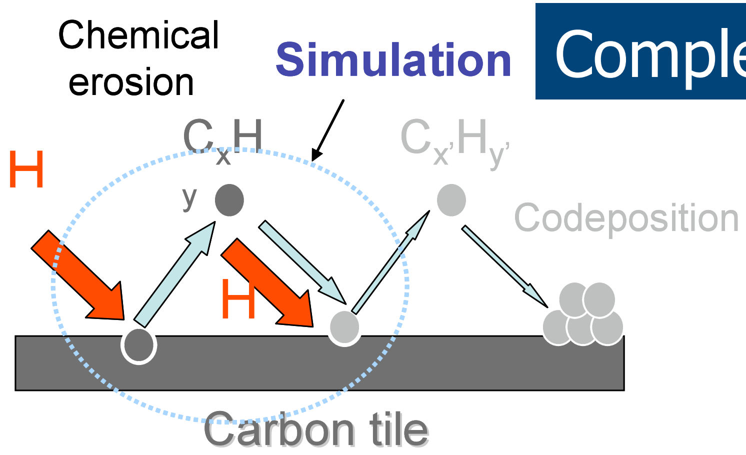

Complex distribution of redeposition species

- Ion species dominate at high temperature
- Neutral species dominate at low temperature

⇒Strong influence of atomic and molecular processes

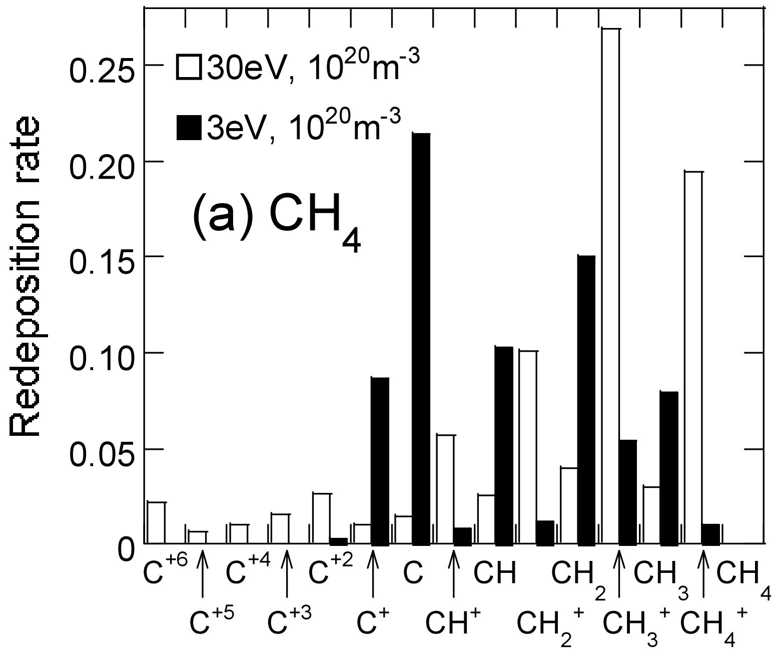

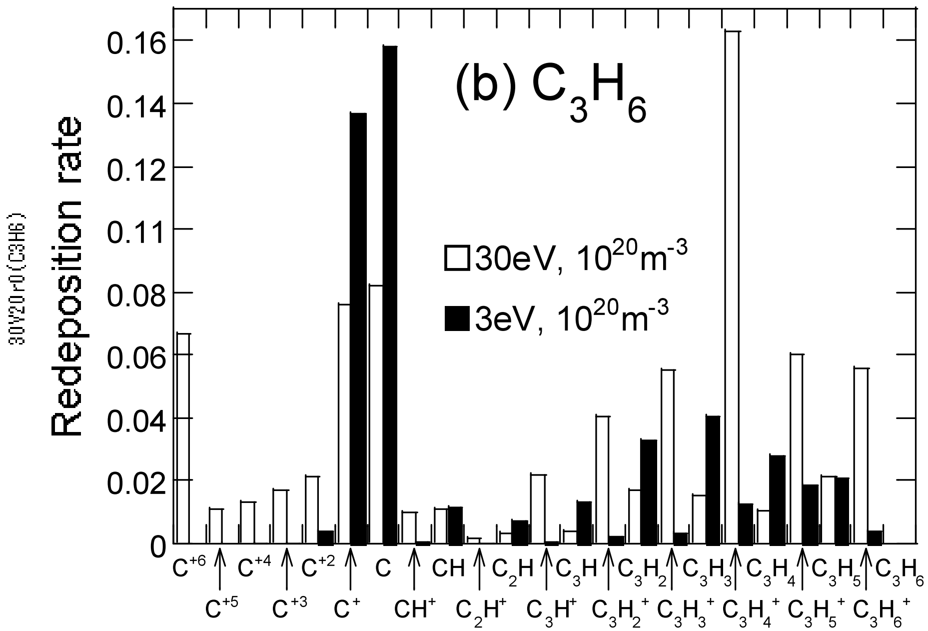

$^{13}CH_4$ injection experiments at TEXTOR

roof-like test limiter exposed to SOL plasma of TEXTOR

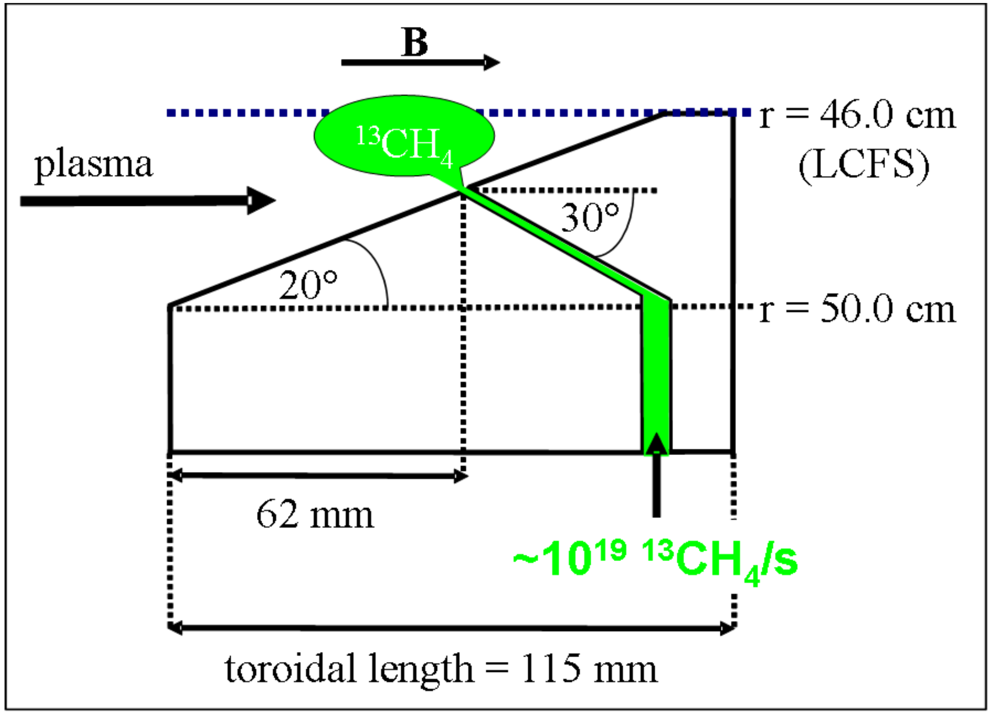

Top of the limiter was positioned at *LCFS*, the radial position of which is *r*=46 cm.

At *LCFS*, T_e=54 eV, T_i=1.5T_e and n_e=1.9x10^{12} cm^{-3}.

Radial decay of the plasma parameter: l_{Te}=l_{Ti}=40 mm, and l_{ne}=22 mm

$^{13}CH_4$ was injected into the plasma through a hole in the limiter surface.

^{12}C concentration of the background plasma was taken to be 3%. (Assumption)

Most unexpected observation was the very low local deposition of ^{13}C on the limiter surface (~0.2%).

Impurity transport, erosion and deposition process in EDDY and ERO codes were compared to be benchmarked against the experiments.

Observed 2D patterns of ^{13}C deposition *on* the surface

Kreter et al.

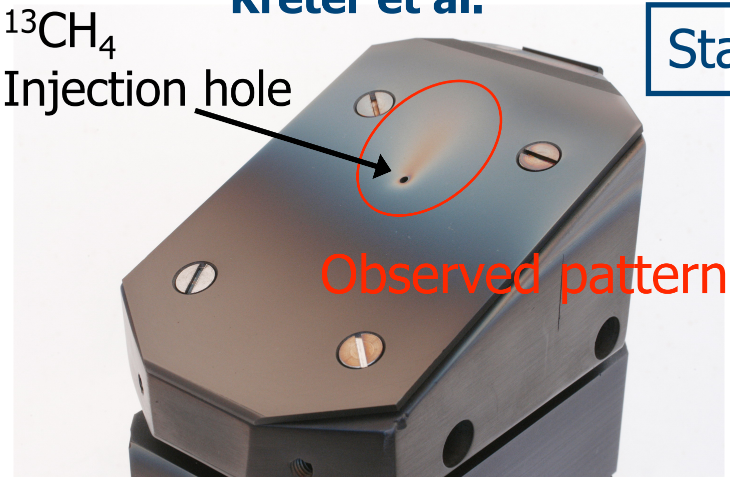

Standard condition: S=0.5 and Y_{chem}=3%

For both EDDY and ERO:

~50% depsoition efficiency

– a factor of 100 larger than in experiment

Very localized deposition pattern (too much peaked)

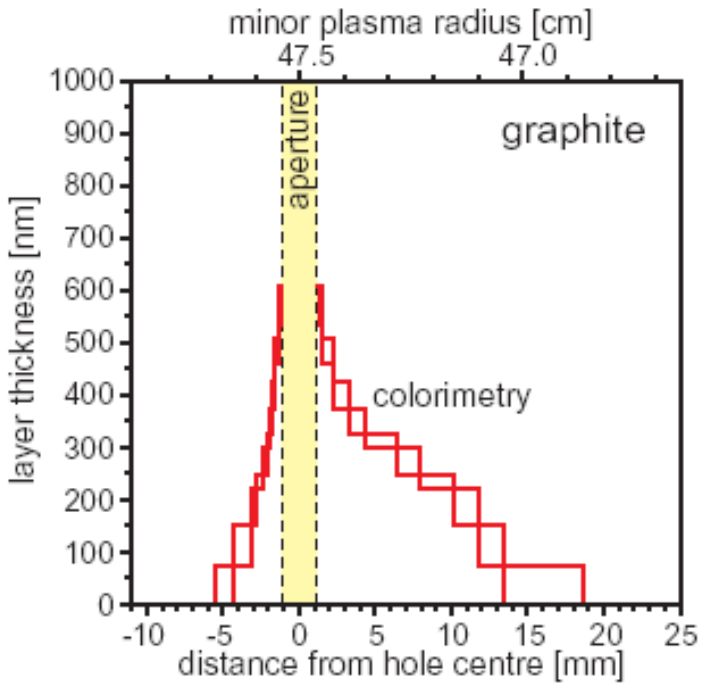

S=0.5, but enhanced erosion of redeposited carbon atoms, Y_{enh}=30%

EDDY: 33% ^{13}C depsoition
ERO: 32% ^{13}C depsotion

Still too large ^{13}C depsoition and patterns still too much peaked

S=0 (or small) & Enhanced erosion **?**

Dynamics of ^{13}C deposition efficiency (EDDY)

Deposition efficiency strongly changes with injection time.

With increasing injection time, deposition efficiency strongly decreases due to increasing re-erosion of the redeposited ^{13}C.

With further increasing time, deposition efficiency approaches a steady state value due to smaller change in the ^{13}C concentration.

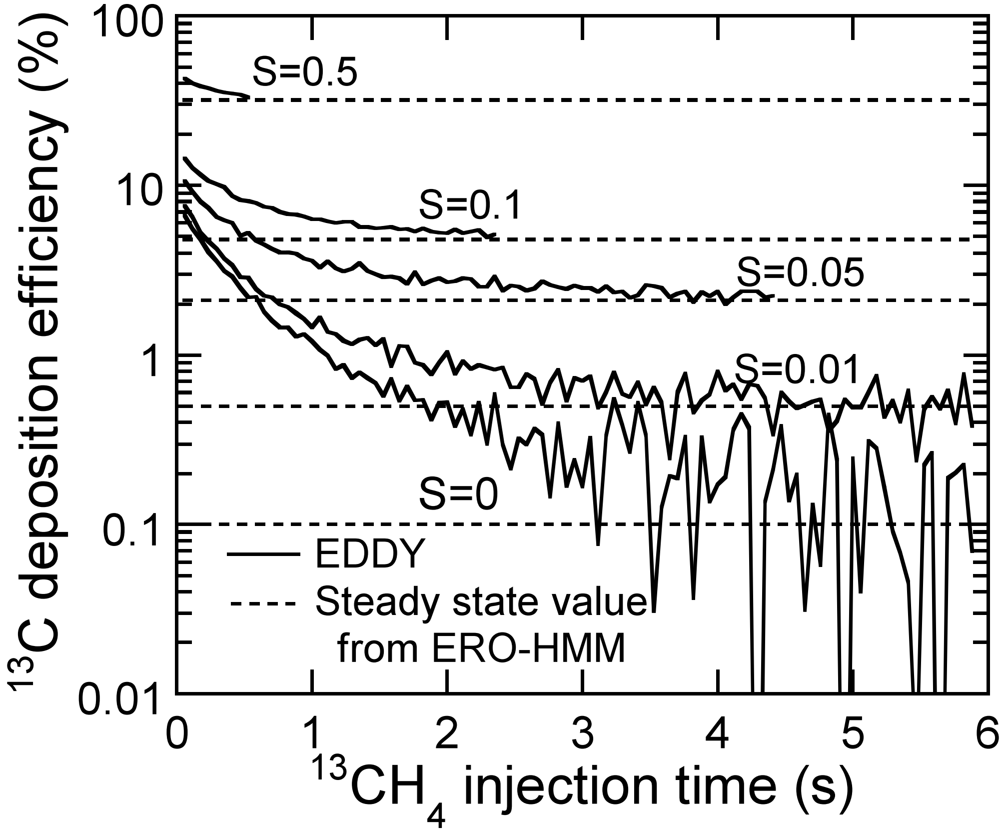

Deposition efficiency in steady state is in fair agreement with the efficiency calculated by ERO-HMM, not only for S=0 but also for S=0.01-0.5.

Injection time (5.88 s) is much shorter than by the experiment (108 s).

A steady state condition is reached during the modeled injection.

(B) MODELLING AND INTEGRATED SIMULATION

a) Projectile reflection and physical sputtering

b) Chemical sputtering and hydrocarbon emission

c) Impurity deposition and collisional mixing

d) Thermal diffusion of impurities in materials

e) Impurity transport in near-surface plasmas

f) Molecular dynamics simulation of particle solid interactions

g) Particle-in-cell simulation of plasma/sheath on surfaces

Classical molecular dynamics (MD) simulation

The force on each atom is calculated from the analytical derivation of the interaction potential.

Potential for W-C-H system

$$V = \sum_{i>j} f_{ij}^{c}(r_{ij})\left[V_{ij}^{R}(r_{ij}) - \frac{b_{ij}+b_{ji}}{2}V_{ij}^{A}(r_{ij})\right]$$

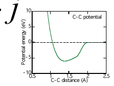

Juslin et al.

Repulsive term : $V^{R}(r) = \dfrac{D_0}{S-1}\exp\left(-\beta\sqrt{2S}\,(r-r_0)\right)$

Attractive term : $V^{A}(r) = \dfrac{SD_0}{S-1}\exp\left(-\beta\sqrt{2/S}\,(r-r_0)\right)$

Cutoff-function : $f^{c}(r) = \begin{cases} 1, & r \le R-D, \\ \frac{1}{2} - \frac{1}{2}\sin\left(\frac{\pi}{2}(r-R)/D\right), & |R-r| \le D, \\ 0, & r \ge R+D \end{cases}$

repulsive force

attractive force

Bond-order function : $b_{ij} = \left(1+\chi_{ij}\right)^{-\frac{1}{2}}$

Many-body term $\chi_{ij} = \sum_{k(\neq i,j)} f_{ik}^{c}(r_{ik})\,g_{ik}(\theta_{ijk})\,\omega_{ijk}\exp\left[2\mu_{ik}\left(r_{ij}-r_{ik}\right)\right]$

Angular function : $g(\theta) = \gamma\left(1 + \dfrac{c^2}{d^2} - \dfrac{c^2}{d^2 + (h+\cos\theta)^2}\right)$

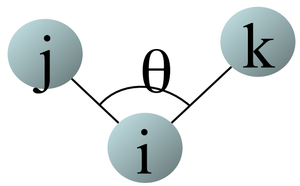

Integrating equation of motions of constituent atoms

Verlet algorithm：

$$\mathbf{r}_j(t+\Delta t) = \mathbf{r}_j(t) + \Delta t\dot{\mathbf{r}}_j(t) + \frac{\Delta t^2 \mathbf{F}_j(t)}{2m}$$

$$\dot{\mathbf{r}}_k(t+\Delta t) = \dot{\mathbf{r}}_k(t) + \frac{\Delta t}{2m}\left\{\mathbf{F}_k(t+\Delta t) + \mathbf{F}_k(t)\right\}$$

Verlet algorithm is simple and high accuracy.

Coupling to an external bath (Langevin equation)

$$\lambda = \sqrt{1 + \frac{\Delta t}{\tau_T}\left(\frac{T_0}{T} - 1\right)}$$

Δt ： time step, τ_T ： time constant
T ： temperature of the system, T_0 ： fixed reference temperature

It represents a proportional scaling of the velocities per time step.

Periodic boundary condition

The simulation cell is replicated throughout the space to form an infinite lattice.
If an atom leaves the simulation cell, one of its images will enter through the opposite side.

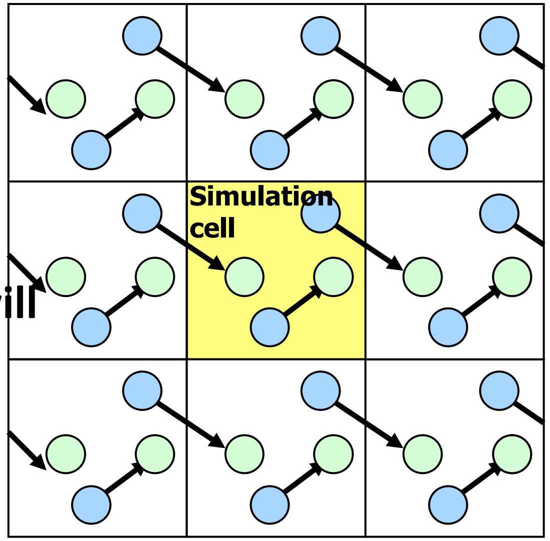

Simulation cell： should be large → **More realistic, but time-consuming.**

Surface Erosion and Carbon Deposition on Tungsten

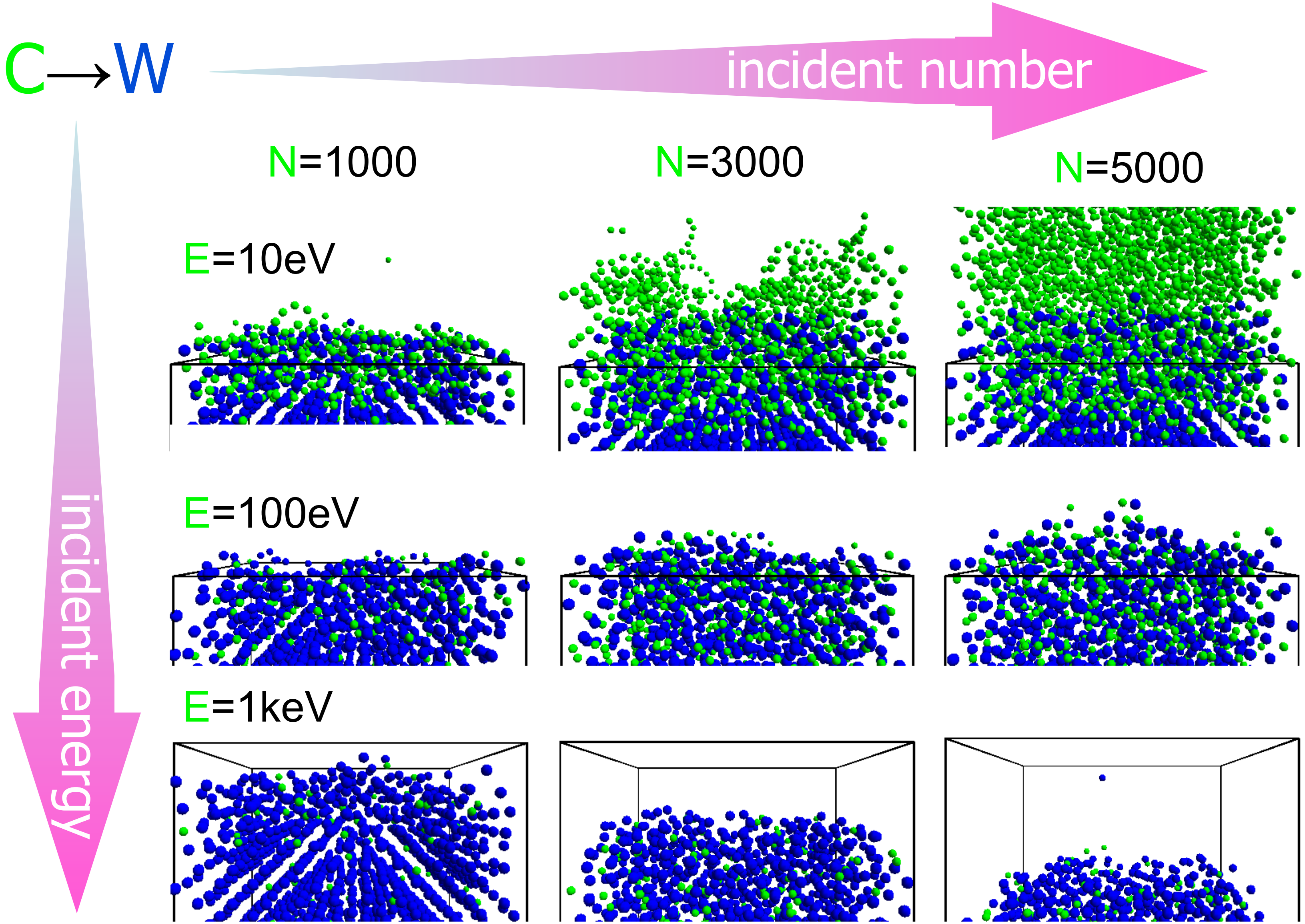

Preparation of Realistic PFW Surfaces

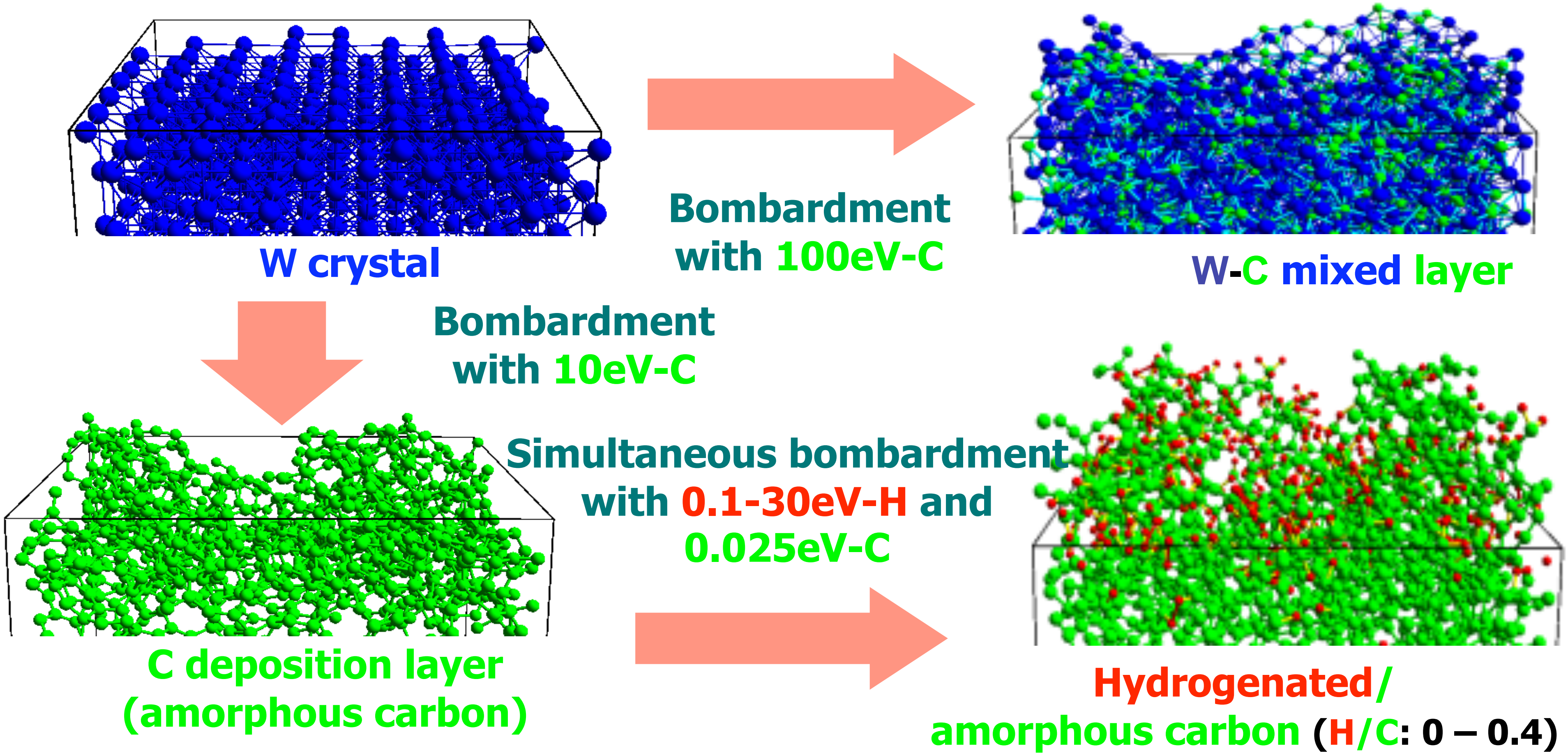

- The W surface is bombarded with C atoms at the temperature of 10eV and 100eV.
- At low plasma temperature, the W is covered by deposited C and at higher temperature **W-C mixed layer** is formed.
- The **a-C:H layer** with different H/C is formed after a-C is bombarded with H atom.

Reflection coefficient and reflected species

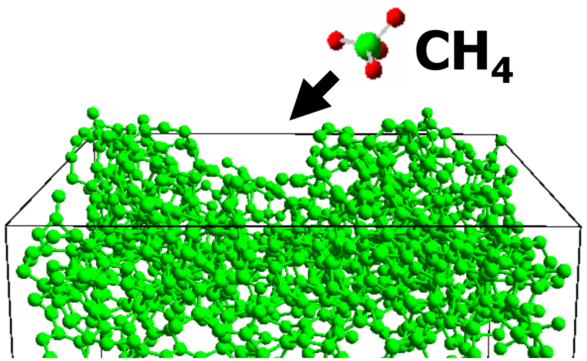

amorphous carbon

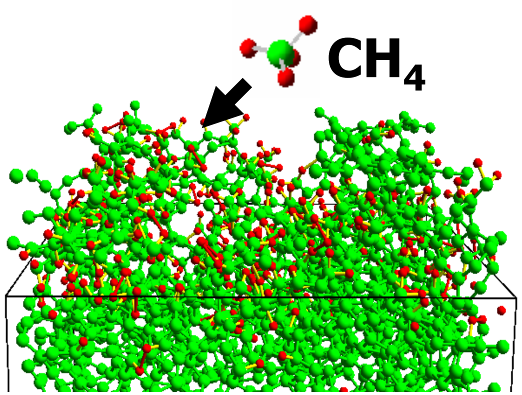

a-C:H

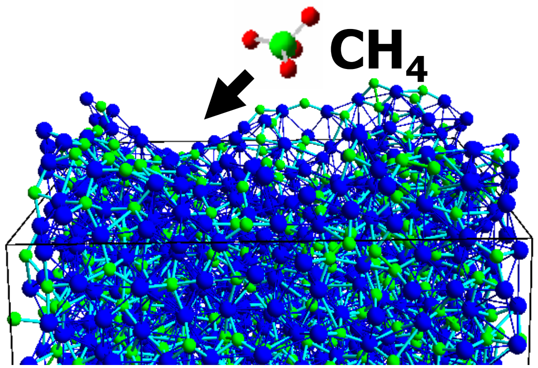

W-C mixed layer

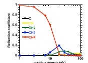

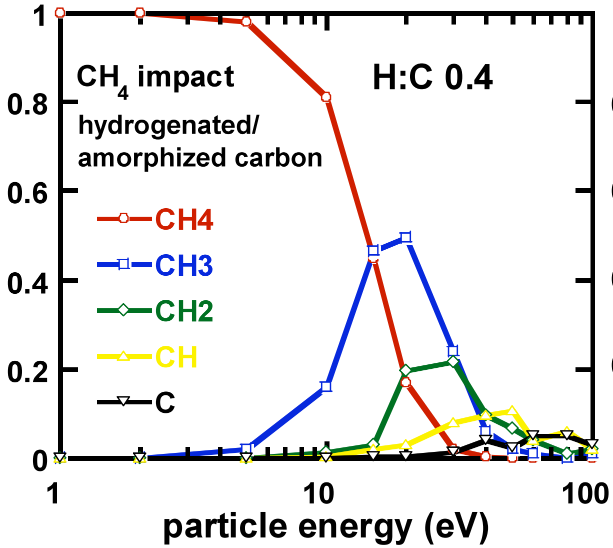

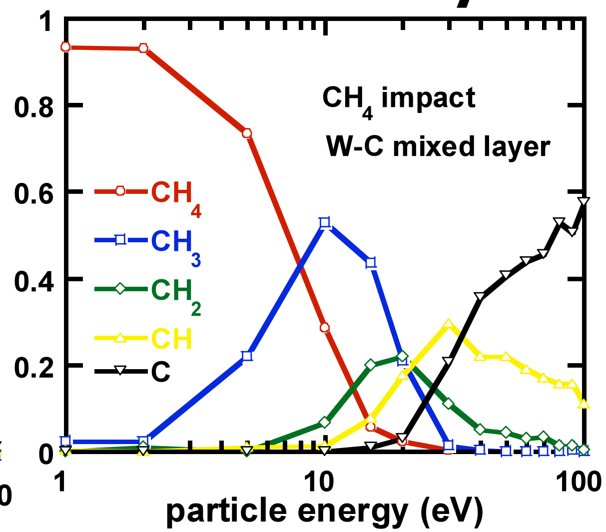

- Most of incident methane reflect at thermal energy and sticks at higher energy (>10eV).
- High hydrogen content in amorphous carbon increases the reflection coefficients.
- The W surface more increases the reflection coefficient and there reflected much more C atoms.

Sticking/reflection of hydrocarbons at PFWs

Incident species dependence of reflection coefficient

Incident at CH_y(y=0～4)

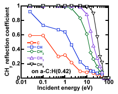

Incident at C_2H_y(y=0～6)

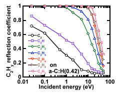

(B) MODELING AND INTEGRATED SIMULATION

a) Projectile reflection and physical sputtering

b) Chemical sputtering and hydrocarbon emission

c) Impurity deposition and collisional mixing

d) Thermal diffusion of impurities in materials

e) Impurity transport in near-surface plasmas

f) Molecular dynamics simulation of particle solid interactions

g) Particle-in-cell simulation of plasma/sheath on surfaces

Particle-in-Cell (PIC) Simulation of Plasma and sheath

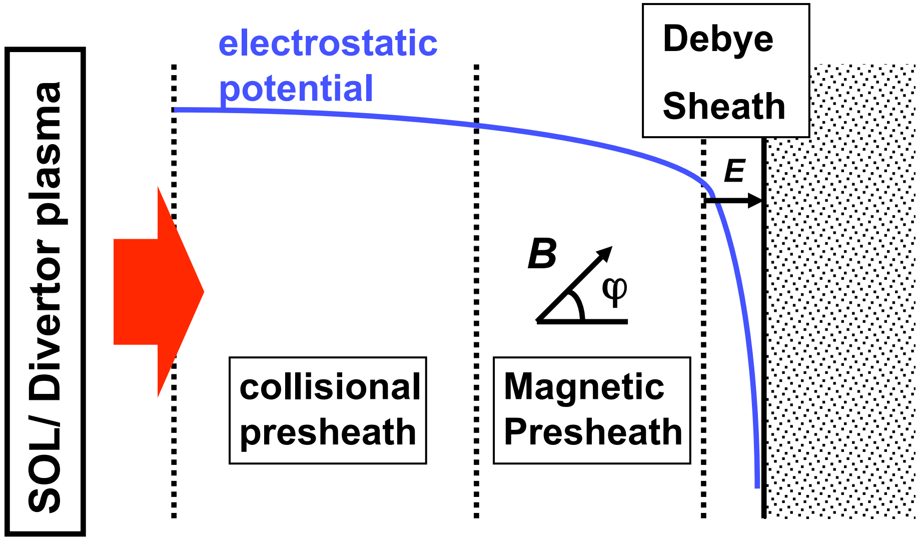

- Plasmas in the fusion devices are usually contacting with walls.
- Sheath layer is formed in front of wall.
- MP and DS region is simulated.

PIC simulation

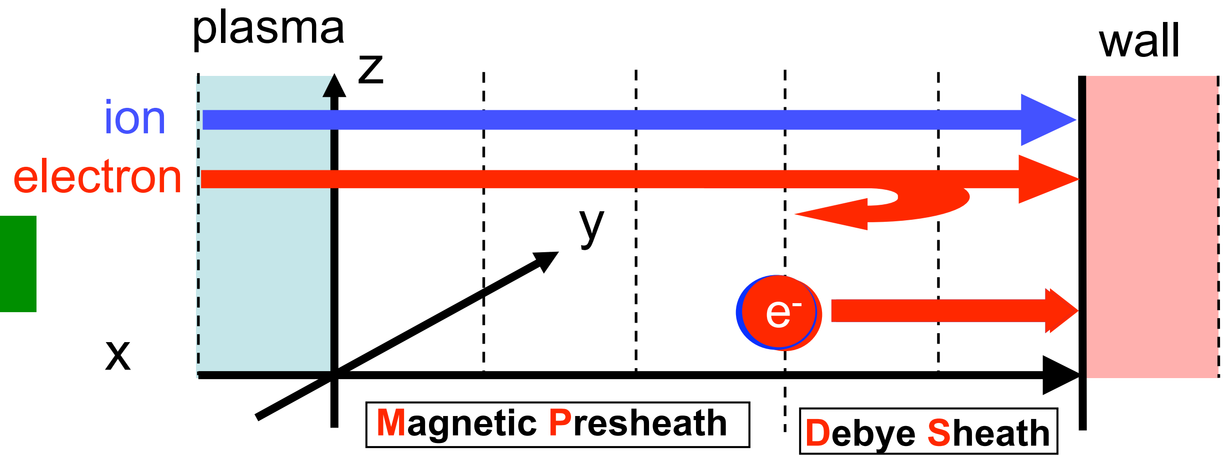

- PIC code solves the equations of motion and Poisson's equation self-consistently.
- The plasma particles with Maxwellian velocity distribution are generated at the edge region.
- The sheath potential vary with the charging of the wall.

Sheath Potential Profiles with Oblique Magnetic Field

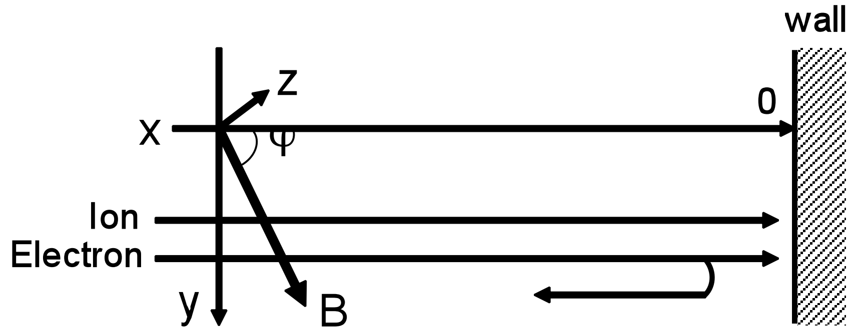

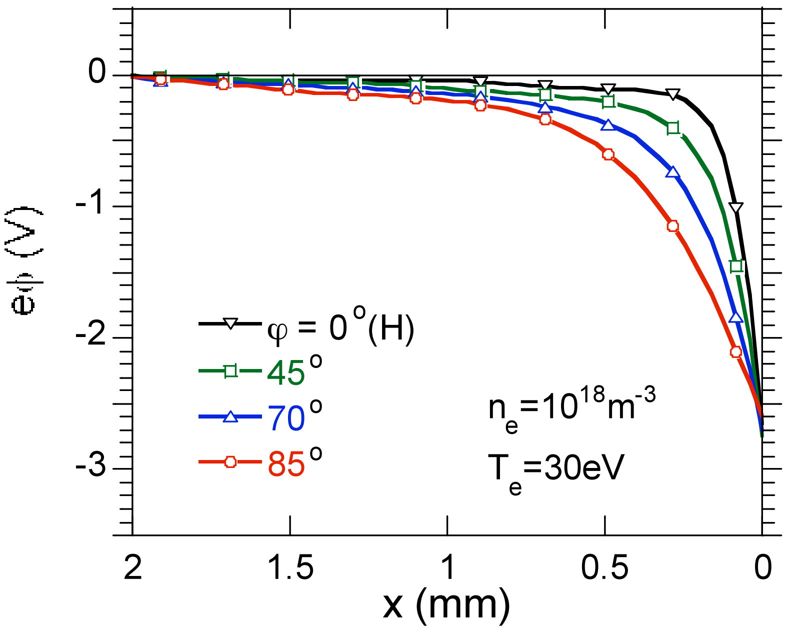

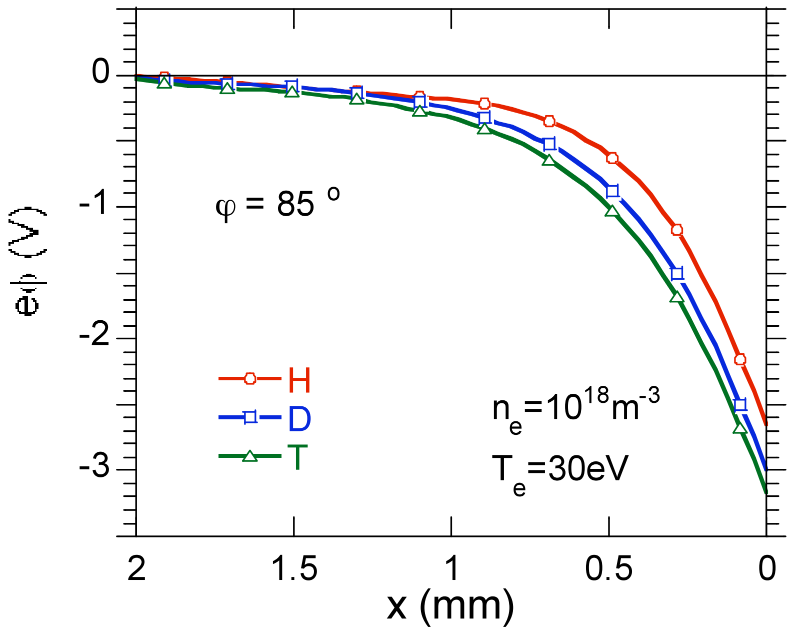

- The magnetic presheath is formed due to the polarization between ions and electrons.
- When the magnetic field is almost parallel to the surface, the width of MP increases.
- The heavier hydrogen isotopes have larger Larmor radius, the width of MP increases.

Energy and angular distributions of ions incident on PFW

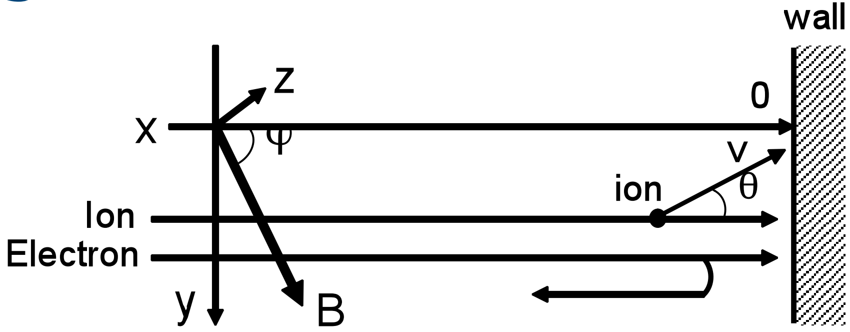

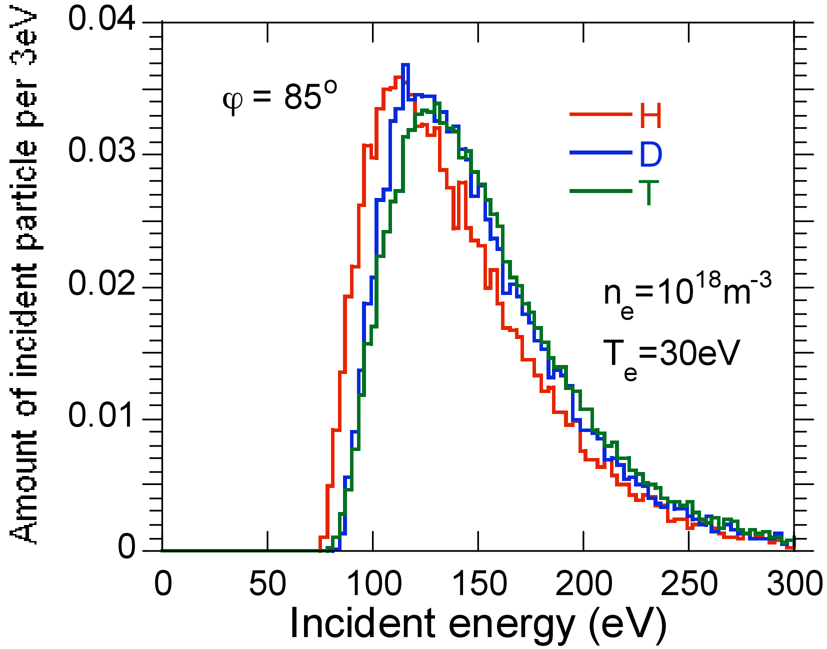

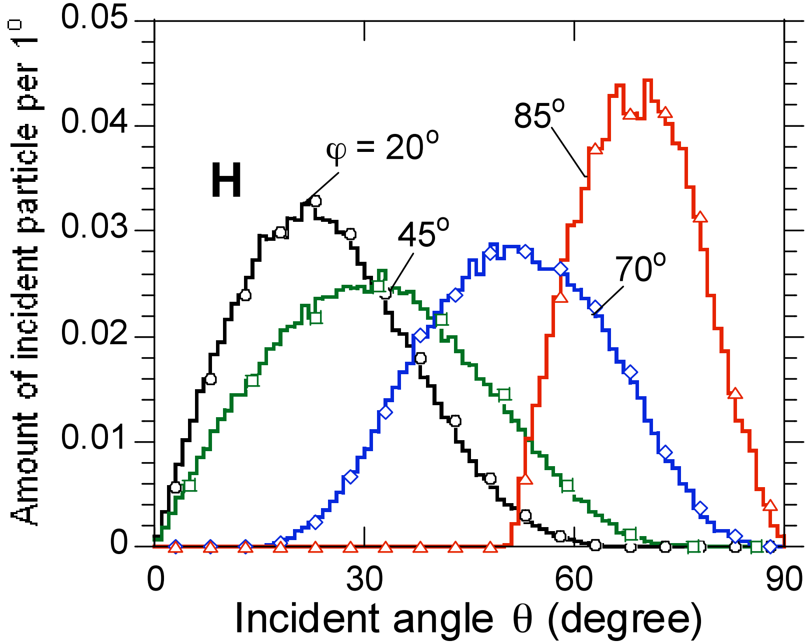

- The impact energy does not depend on angle of magnetic field because potential drop is same.
- The energy .
- The most for the case of the

The energy and angular distributions affect the sputtering and the reflection from the wall

2D-PIC simulation of plasma penetrating into Gaps

$T_e = T_i = 10eV$,

$n_0 = 10^{18} m^{-3}$

■ W_G=1mm

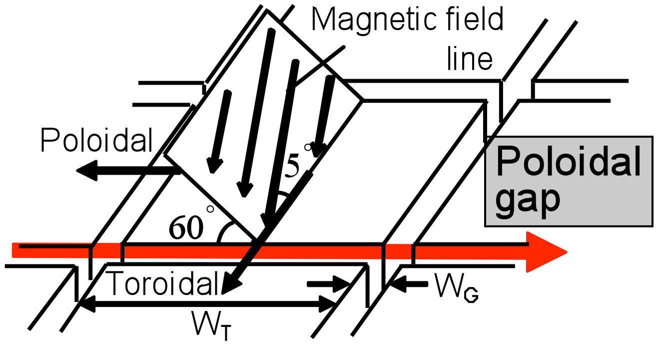

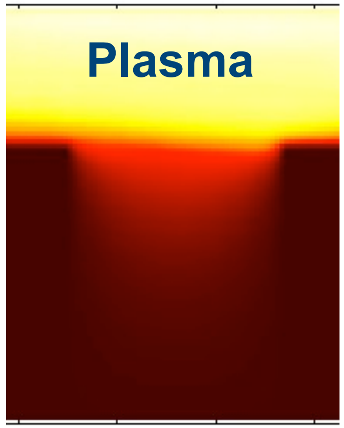

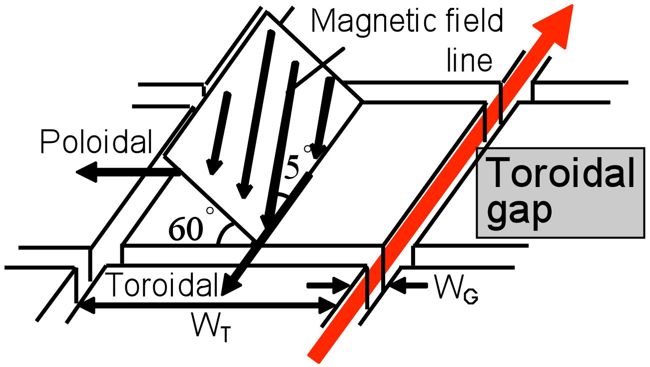

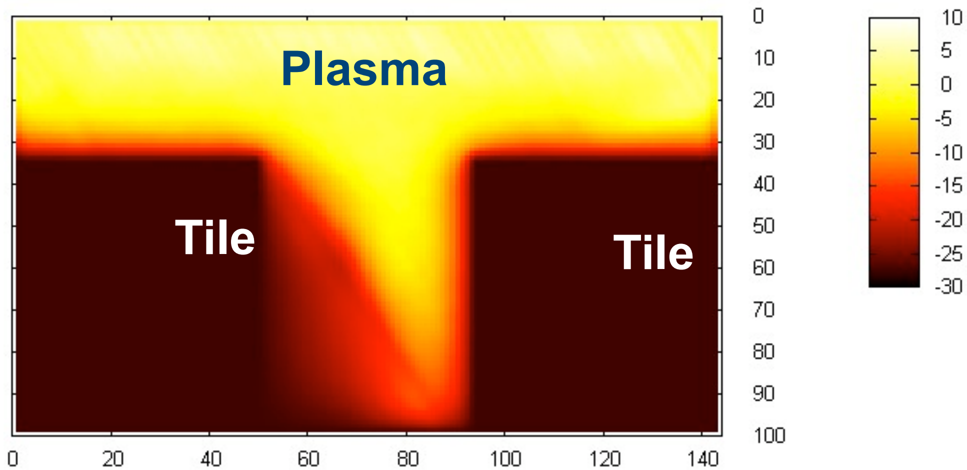

Plasma and sheath profiles in the toroidal gap

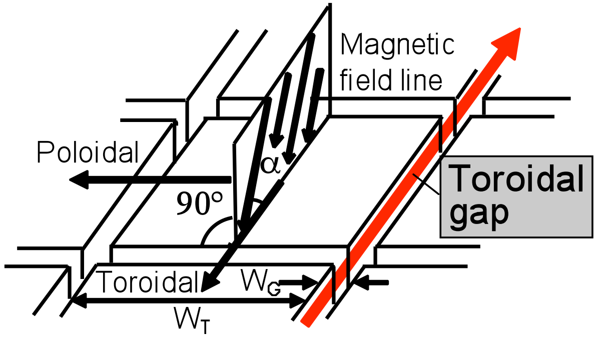

- Magnetic field line is only inclined by 5° with respect to the toroidal direction.

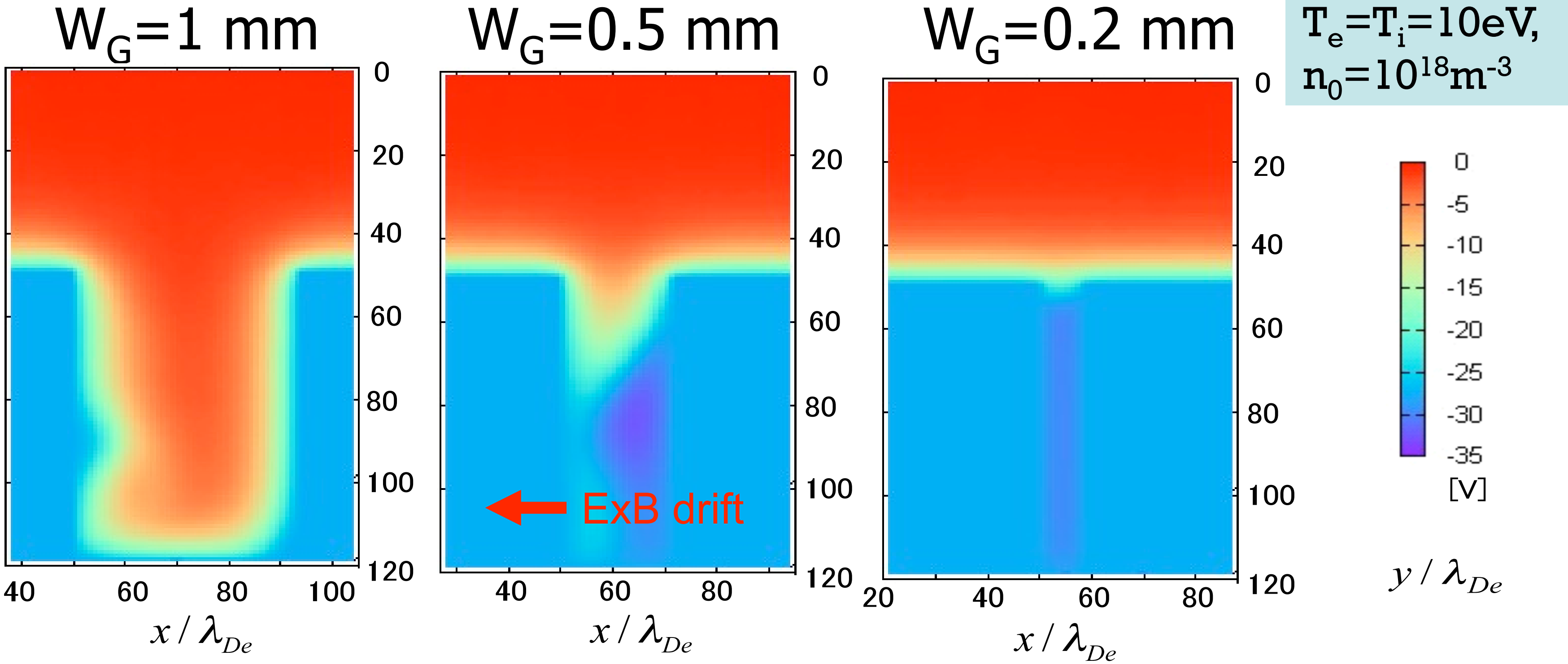

- plasma particles can penetrate into a wide gap of 1mm.
- H ion with gyro radius of 0.1mm cannot penetrate into a narrow gap of 0.2mm.
- When the gap width is 0.5mm, H ion cannot deeply penetrate due to E x B drift.

Penetration depth of hydrocarbons in the toroidal gap

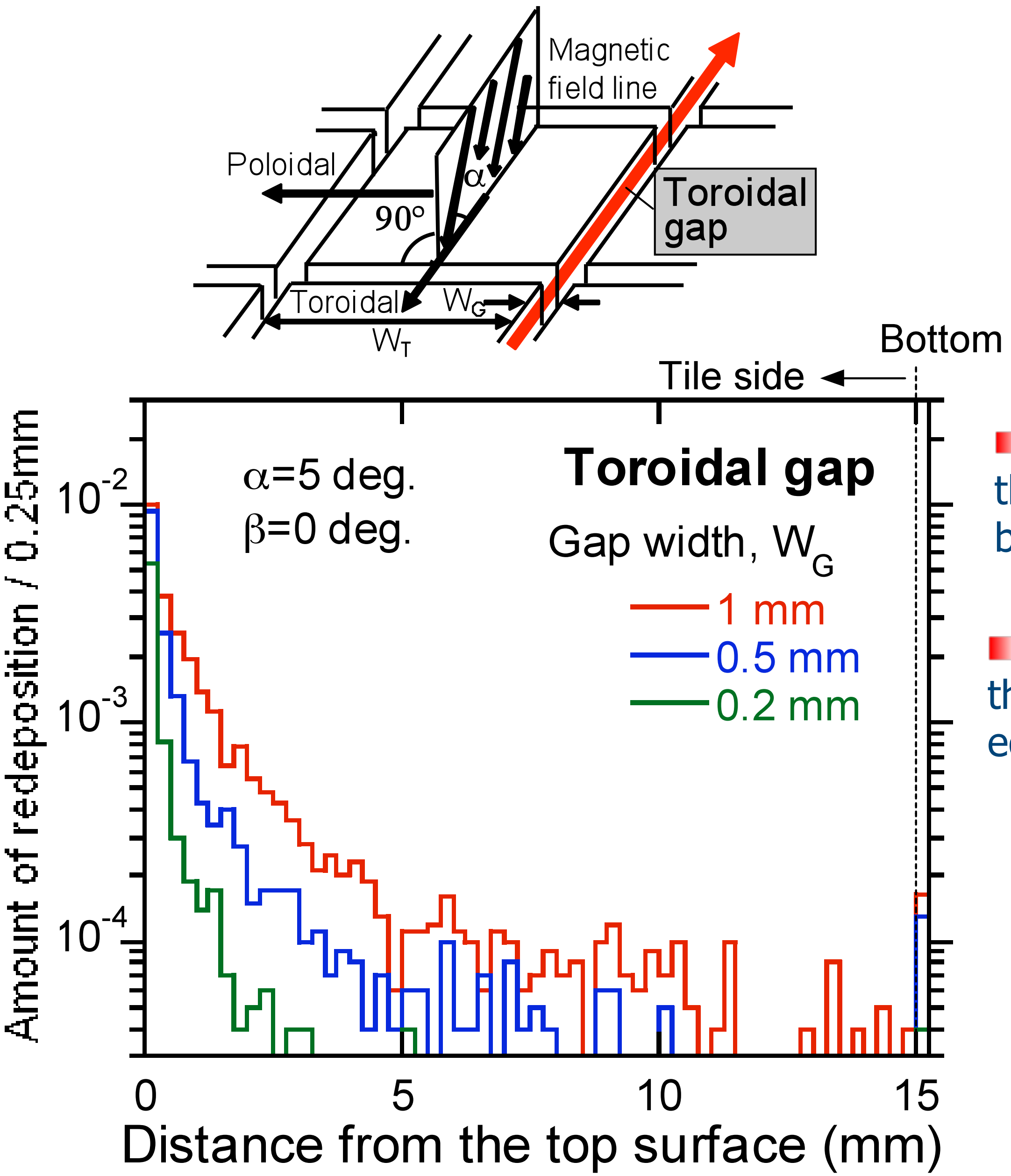

- When the gap width is 0.5 mm or more, the redeposition can be found at the bottom of the gap.
- Very narrow gap (<0.2 mm) causes the redeposition localized at the gap edge.

Deposition profiles of hydrocarbons at the gap sides

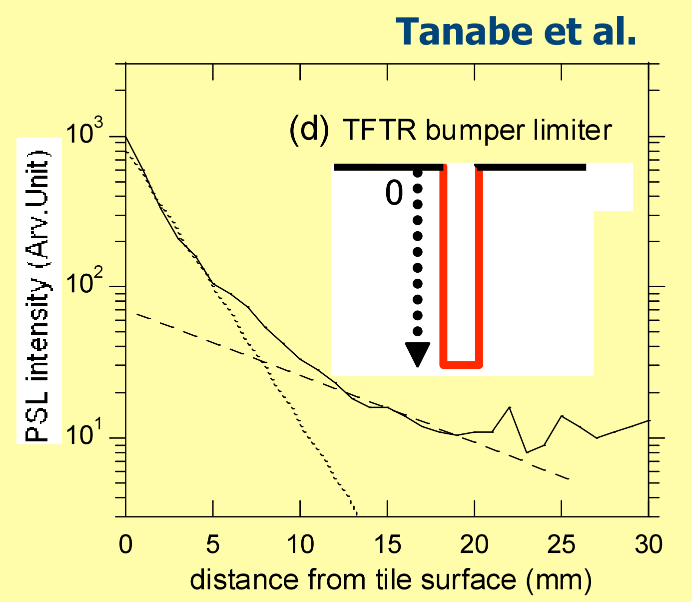

Effect of reflection

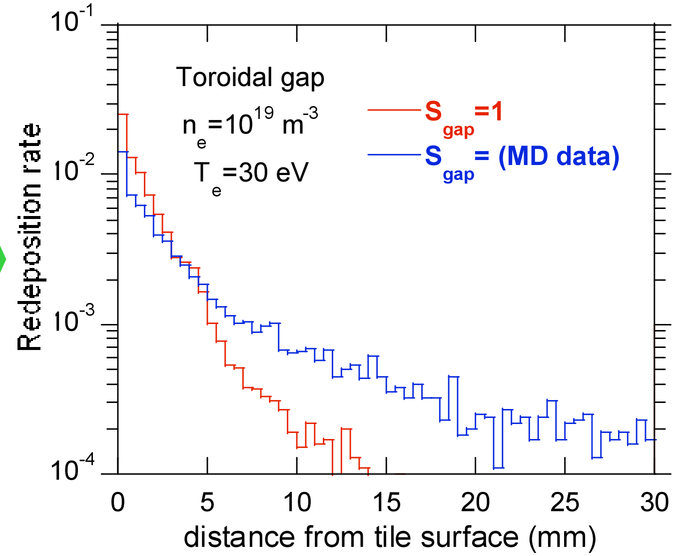

Species dependence

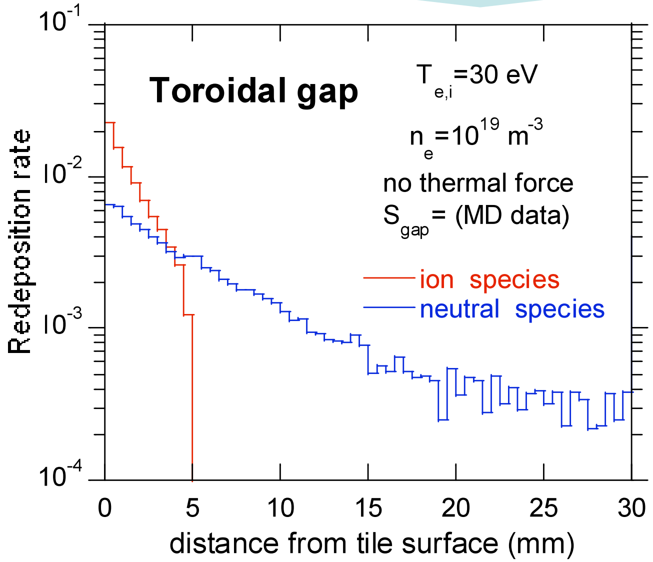

- Using sticking coefficient calculated by MD, low energy hydrocarbons are reflected repeatedly.
- The neutral species are liberated from a magnetic constrain, they are redeposited deeply.
- Since the ionized particles are confined by the magnetic field and have high sticking coefficient due to sheath acceleration, they are redeposited in the gap edge.

Carbon Deposition in the gaps of castellated tiles

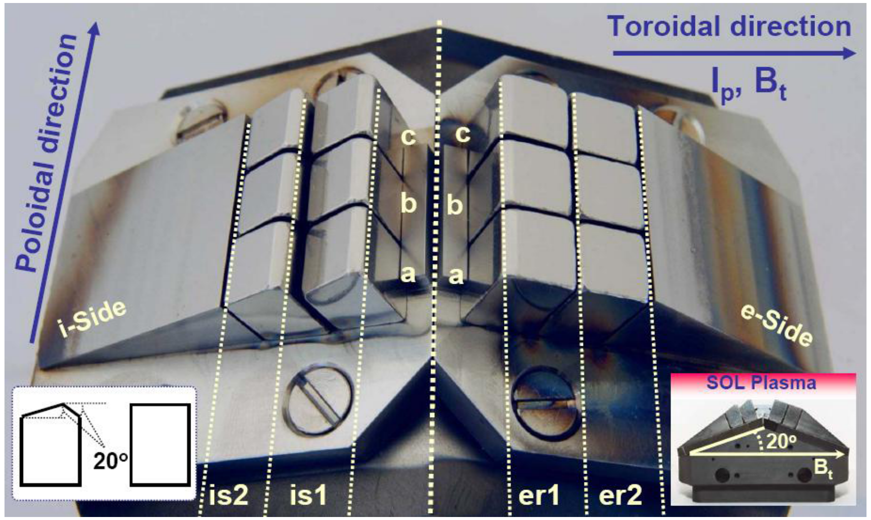

(Castellation tile used in TEXTOR)

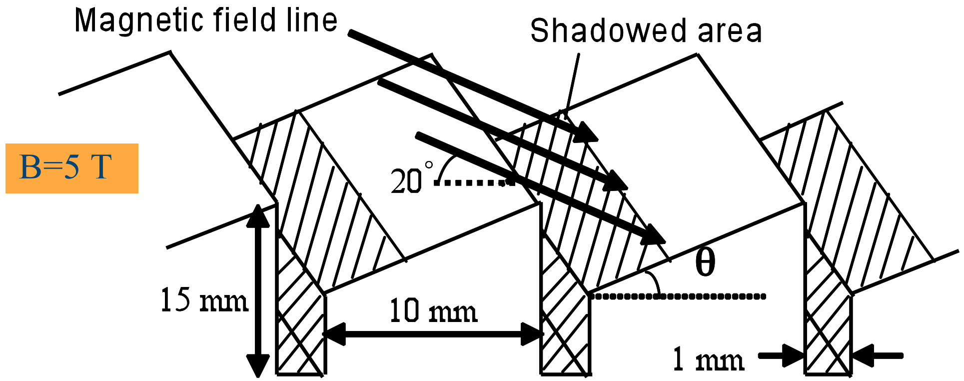

- Experiments with an ITER-like castellation geometry in TEXTOR, are studying the fuel retention and impurity transport in gaps (Litnovsky et al.).
- In order to compare between the experiment and the simulation, we performed a simulation study of the plasma penetration and transport of hydrocarbon.
- The plasma hydrogen ions with the maxwellian velocity distribution move along the magnetic field lines with gyration and bombard the model structure. A CH_4 molecule is released from the point bombarded by hydrogen ion.
- The tile surface is inclined for varying the shadowed area.

Comparison between experimental and simulated results

We compared between TEXTOR experiment and simulation.
The hydrocarbon sputtered chemically and carbon sputtered physically are emitted from surface.

Litnovsky et al.

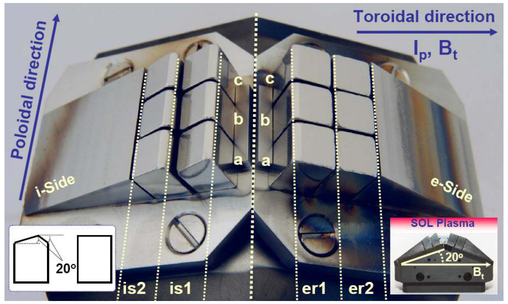

$W_T = 10$ mm,

$n_e = 6\text{x}10^{18}\ \text{m}^{-3}$,

$T_e = 20$ eV,

$B = 5$ T

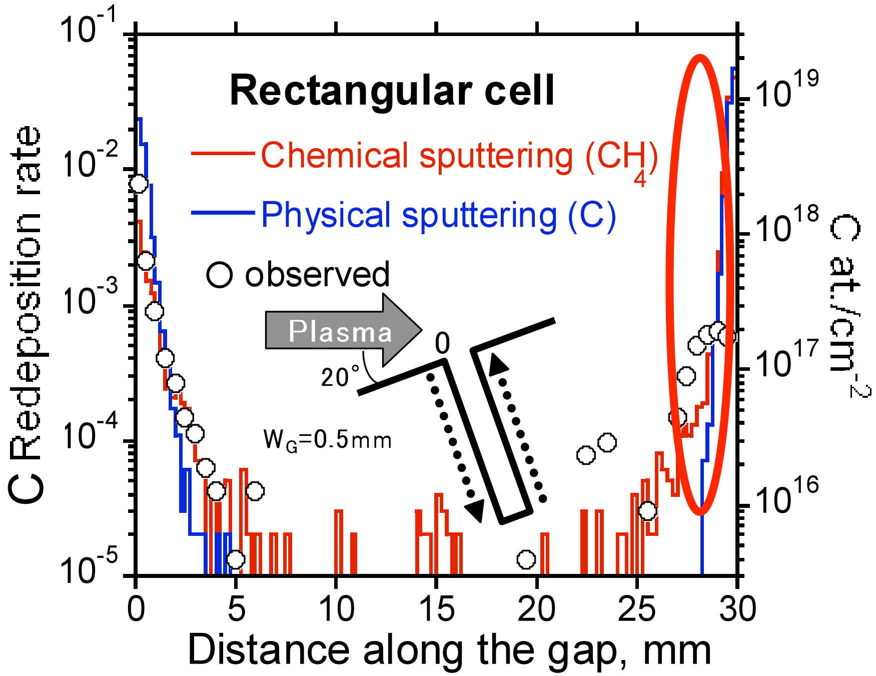

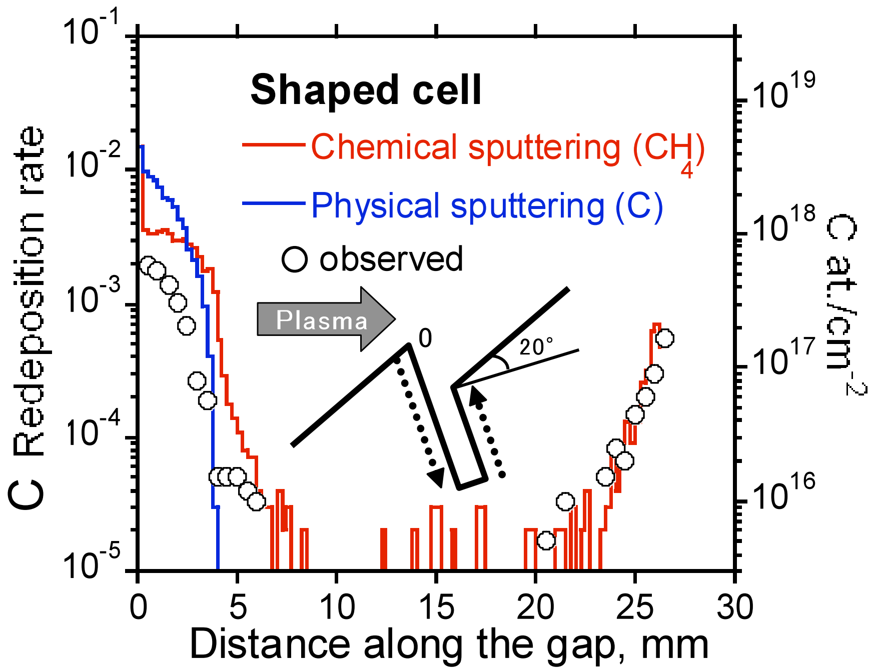

- The calculated redeosition profiles reproduce the experimental profiles of C deposition.
- The redeposition layer is re-eroded by the bombardment of background plasma, therefore, C deposition is reduced at the gap edge of the rectangular cell.

Conclusions

(I) "Erosion/deposition" on plasma facing walls in fusion devices is a critical issue related to
- (a) global transport of impurities in plasma boundary,
- (b) lifetime of plasma-facing components and
- (c) tritium retention in plasma-facing components.

(II) Modelling codes of "erosion/deposition" require to treat self-consistently:
- (a) Physical and chemical erosion ***of*** surface,
- (b) Transport of released impurities ***above*** surface,
- (c) Redeposition of returning impurities ***on*** surface and
- (d) Resultant material mixing ***below*** surface

(III) Models and assumptions in the codes have to be evaluated in cross-code and code-experiment benchmarking,
whereas reliable database of physical parameters used in codes have to be prepared.

Conclusions

(continued)

(IV) Particle-in-cell (PIC) simulation of plasma and sheath above the PFW surface should be incorporated in “erosion/deposition” codes to analyze geometry effects such as gaps in the castellated tile.

(V) In addition to existing static and dynamic Monte Carlo codes of plasma wall interactions, classical molecular dynamics (MD) simulation is an effective tool to analyze “erosion/deposition”. **But, it requires formalism of realistic interaction potentials and high performance computing.**

(VI) Integration of “erosion/deposition” codes with SOL/Divertor simulation codes is an urgent issue for understanding of plasma wall interactions in fusion devices in more realistic in-vessel geometry.

THANK YOU
for your attention

This work was supported by the Grant-in-Aid for Scientific Research on Priority Areas "***Tritium Science and Technology for Fusion Reactor***" of the Ministry of Education, Culture, Science and Technology in Japan

Scientific Research in Priority Areas
Tritium for Fusion
2007 - 2011